Digital Control and Power Systems for the PEGASUS-III Experiment

Michael W. Bongard, Michael T. Borchardt, Stephanie J. Diem, Raymond J. Fonck, John A. Goetz, Armand K. Keyhani, Benjamin A. Kujak-Ford, Benjamin T. Lewicki, Mark D. Nornberg, Jilliann K. Peery, Christopher Pierren, Joshua A. Reusch, Nathan J. Richner, Carolyn E. Schaefer, Aaron C. Sontag, and Justin D. Weberski

***Abstract*— The PEGASUS-III experiment is a solenoid-free, low aspect ratio spherical tokamak that will serve as a dedicated U.S. platform for comparative nonsolenoidal tokamak plasma startup studies. Approximately 175 megavolt-ampere (MVA) of reconfigured and expanded programmable power systems, 7 MJ of new stored energy, and new digital control and protection systems for the facility are being commissioned to support PEGASUS-III upgrades. These include: increased toroidal field (0.15–0.6 T); new divertor and poloidal field coils; increased pulse length; local and coaxial helicity injectors for solenoid-free plasma initiation; radio frequency (RF) systems for heating and current drive; and a diagnostic neutral beam (DNB). A new real-time digital control system implements 16 proportional-integral differential (PID) feedback controllers with 25 kHz loop rates to control the electromagnets and helicity injectors. The poloidal field coils, helicity injector arc currents, and toroidal field are driven by 36 3.6 MVA (4 kA, 900 V) insulated-gate bipolar transistor (IGBT) buck converters. Helicity injector bias voltage and current will be provided by a set of four 10.8 MVA multilevel buck converters (MLBCs). Each is comprised of an 1800 V integrated gate-commutated thyristor (IGCT) stage and a ±900 V IGBT stage in series, providing controllable $I_{\text{inj}} \leq 4$ kA at $V_{\text{inj}} \leq 2.7$ kV. A field programmable gate array (FPGA)-based digital fault protection system multiplexes controller commands to individual power semiconductors in these supplies, monitors their operational status, and executes shutdown sequences within 10 μs of fault detection. An 80 kV, 4 A zero-voltage-switching (ZVS) resonant converter with <1% output ripple is under development for the DNB and is being evaluated as a topology to drive RF sources.**

***Index Terms*— Digital control, plasma generation, pulse-width modulated power converters, real-time systems, resonant power conversion, tokamaks.**

I. INTRODUCTION

LOW aspect ratio spherical tokamaks (STs) may afford an attractive path to developing compact nuclear fusion reactors. However, the limited physical space in the configuration's central column as the aspect ratio is reduced increasingly precludes space for a conventional Ohmic solenoid for plasma initiation and sustainment [1], [2]. Accordingly, robust solenoid-free startup techniques are expected to be required for future nuclear-grade STs [3]. Their availability would also be highly desirable for advanced tokamaks as well, for example, by freeing valuable inboard space for additional breeding volume or high-field-side actuators.

The PEGASUS-III experiment is a major upgrade to the ultralow aspect ratio PEGASUS ST [4] that is under construction and commissioning at the University of Wisconsin-Madison, Madison, WI, USA. It will serve as a dedicated U.S. platform for comparative solenoid-free tokamak startup studies. Upgraded features include: a factor of 4 increase in the toroidal field B_T; new divertor coils; longer pulse length; a new diagnostic neutral beam (DNB); and no central solenoid in the central column. Its nominal machine and plasma parameters are: major radius $R_0 \leq 0.48$ m, aspect ratio $A \geq 1.22$, plasma current $I_p \leq 0.3$ MA, $B_T \leq 0.6$ T, and $\Delta t_{\text{pulse}} \sim 0.1$ s. Sontag *et al.* [5] provides additional information regarding the upgraded facility.

PEGASUS-III will be equipped with multiple solenoid-free startup systems to compare, contrast, and combine suitable techniques. These include local helicity injection (LHI) [6], coaxial helicity injection (CHI) [7]–[9], and radio frequency (RF) sources for electron cyclotron and electron Bernstein wave heating and current drive [3].

Experiments on the facility are enabled by modular, high-power, switching power supplies acting under pulse-width modulation feedback control. These supplies are powered by approximately 7 MJ of stored energy in electrolytic capacitor banks. A resonant converter system powers the DNB and is being evaluated for suitability with the RF sources.

This article describes these power supplies, their stored energy and its management, and the associated control and protection systems being fielded for initial PEGASUS-III operations. Section II provides an overview of the power systems in the facility and their initial configuration for first experiments. Control and protection systems are detailed in Section III. Section IV describes the buck converters retained from PEGASUS and expanded for PEGASUS-III. A new multilevel buck converter for helicity injection bias is detailed in Section V. The zero-voltage-switching (ZVS) resonant converters for the DNB and RF are described in Section VI. It is concluded in Section VII.

II. POWER SYSTEMS OVERVIEW

Power systems and their associated stored energy are located in five designated switchyard lockout areas in the

Manuscript received 28 January 2022; revised 30 March 2022; accepted 1 April 2022. Date of publication 3 May 2022; date of current version 30 November 2022. This material is based upon work supported by the U.S. Department of Energy, Office of Science, Office of Fusion Energy Sciences, under Award Numbers DE-SC0020402 and DE-SC0019008. The review of this article was arranged by Senior Editor G. H. Neilson. *(Corresponding author: Michael W. Bongard.)*

The authors are with the Department of Engineering Physics, University of Wisconsin-Madison, Madison, WI 53706 USA (e-mail: mbongard@wisc.edu).

Color versions of one or more figures in this article are available at https://doi.org/10.1109/TPS.2022.3165694.

Digital Object Identifier 10.1109/TPS.2022.3165694

TABLE I
PEGASUS-III SWITCHYARD ALLOCATION

Yard	Drives	Topology
1	Electromagnets	Buck Converter
2	LHI, S-CHI	Multi-level Buck Converter
3	T-CHI	Low Inductance Capacitor Bank
4	DNB	ZVS Resonant Converter
5	RF Sources	ZVS Resonant Converter

PEGASUS-III experimental hall. As denoted in Table I, the switchyards are sited to be proximate to their intended loads, stored energy, and are clustered by function. Apart from the designated output transmission lines to the loads, switchyards are electrically isolated from the remainder of the facility. They contain their own stored energy, charge/dump infrastructure, and power converters. All systems are precluded from energization when personnel are in the hall via a keyed interlock system.

Switchyard 1 contains a switch wall with 32 modular 3.6 megavolt-ampere (MVA) buck converters built from insulated-gate bipolar transistor (IGBT) switches in an H-bridge configuration. As detailed in Section IV, each converter supplies up to 4 kA at 900 V. Output transmission lines from the buck converter modules are brought to a patch panel to connect to their electromagnet loads. They are length-matched to balance their output impedance and optimize load sharing when multiple converter modules are operated in parallel.

A 900 V capacitor bank built from individual 450 V, 13 $+30\%/-0\%$ mF United Chemi-Con 36 series electrolytic capacitors is connected to each buck converter. Each such bank is comprised of ± 450 V banks connected in series, with their center-point reference soft grounded.

The 32 capacitor banks in switchyard 1 are charged with monolithic $+450$ V and -450 V charging supplies (Lumina CCHP-6000 series) and isolated from each other via suitable isolation diodes. Dump actuation for the banks is provided via a monolithic dump switch and suitably sized dump resistors that allow the $\sim$5 MJ of stored energy in the switchyard to be dissipated in approximately two minutes.

Switchyard 2 contains switch walls and stored energy to drive the helicity injection systems. Four sets of independently controllable supplies are implemented, which may drive up to four individual LHI injectors or be connected in parallel for planned sustained CHI experiments. Such systems are comprised of a 3.6 MVA LHI arc supply, driven by buck converters of the same make as for the electromagnets, and a separately controlled 10.8 MVA (4 kA, 2.7 kV) multi-level buck converter detailed in Section V.

Stored energy for these supplies is provided by $\sim$2 MJ of electrically floating capacitor banks comprised of 450 V subpanels constructed from the electrolytic capacitors described above. As the helicity injectors must be electrically floating to properly operate, these capacitor banks are arranged in an eight-subpanel, 3.6 kV configuration (2.7 kV for bias and 0.9 kV for the LHI arcs). Each of the eight 450 V stages in the four supplies is charged in parallel by a dedicated, isolated Lumina CCPF-1500 charging supply and has per-bank dump resistors actuated by depletion MOSFETs.

Switchyard 3 is allocated for a transient CHI capacitor bank. It is intended to provide $I \leq 32$ kA at $V \leq 2$ kV for 1–3 ms. Reusch *et al.* [9] provides additional detail on this system.

Switchyards 4 and 5 are for ZVS resonant converters (see Section VI) for the DNB and RF sources, respectively. They are intended to provide 5–10 A at 60–85 kV with low output ripple. Each system uses a modest amount of stored energy whose management is integrated with the converter.

The buck converters in switchyards 1 and 2 are modular and reconfigurable by placing units in parallel to increase the total current drive capability to desired loads. Parallelized modules are driven synchronously during a plasma discharge under the control of a dedicated feedback controller.

A representative allocation of these power systems to support initial PEGASUS-III operations is given in Table II. Sixteen feedback control sets drive the electromagnets (in combinations of up to eight equilibrium field coils and four divertor coils) and LHI startup systems. Unipolar, regenerative (two-quadrant) bridges are deployed on loads where appropriate to minimize cost. Bipolar, regenerative (four-quadrant) bridges are employed for an equilibrium coil set, a radial field set for vertical position control, and a stray field mitigation system.

III. FACILITY CONTROL AND PROTECTION SYSTEMS

The PEGASUS-III facility is operated by a distributed control system implemented in LabVIEW. It provides a unified display for, and control of, stored energy in the facility; input programming for the feedback control systems; timing control; data acquisition management; and fault reporting to machine, diagnostic, and physics operators. Individual subsystems are housed on real-time peripheral component interconnect extensions for instrumentation (PXI) host computers that oversee system-specific data acquisition and field programmable gate array (FPGA) hardware. The subsystems report relevant state information to the operator interface and logging systems via network-hosted shared variables. Three major subsystems are detailed in the following.

A. Stored Energy Management

The stored energy management subsystem is comprised of switchyard-level PXI chassis that each contains a real-time embedded computer, an NI 6225 mixed I/O digitizer, an NI 7813R digital FPGA module, digital fiber-optic converters (Electro Standards Laboratories (ESL) Model 6760), and interface electronics to interconnect plant voltage dividers, charge/dump actuators, and the facility interlock system. Their deployment is schematically shown in Fig. 1 for the case of the helicity injection switchyard.

Voltage divider measurements are routed to the system via shielded CAT7 Ethernet cabling, interfacing with the analog interface electronics. Such cabling is effective at mitigating EMI from switching transients during buck converter operation [10], [11]. These measurements are buffered and driven to the charge control system digitizers and exported for use by other power supply health diagnostics.

Charge control is implemented via fiber-optic signals to an interface circuit affixed to the Lumina charge actuators. This optical link allows the actuators to satisfy the requirement of

TABLE II
INITIAL PEGASUS-III POWER SYSTEM AND CONTROL ALLOCATION

	Load	Max. Voltage [V]	Max. Current [kA]	Number of Modules	Topology [Quadrants]	Number of Switches	Min. Stored Energy [kJ]*	Controlled Power [MVA]
Magnets (8 control sets)	Equilibrium Field 123	900	16	4	2Q	8	336	14.4
	Equilibrium Field 45	900	8	2	4Q	8	168	7.2
	Equilibrium Field 678	900	16	4	2Q	8	336	14.4
	Divertor Set 1	900	16	4	2Q	8	336	14.4
	Divertor Set 2	900	16	4	2Q	8	336	14.4
	Radial	900	4	1	4Q	4	84	3.6
	Toroidal Field	900	48	12	2Q	24	2,784	43.2
	Stray Field Mitigation	900	4	1	4Q	4	84	3.6
Helicity Injection (8 control sets)	LHI Arc (×4)	900	4	1/set	2Q	2/set	84/set [336]	3.6/set [14.4]
	HI Bias (×4)	2,700 (1800 ± 900)	4	2 + SCR crowbar/set	2Q IGBT, 2Q IGCT	6/set	422/set [1,688]	10.8/set [43.2]
	Totals					**104**	**6,488 (min) ~7,000 (avg)**	**172.8**

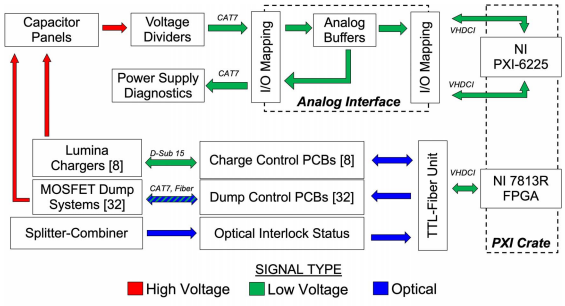

Fig. 1. Block diagram of PEGASUS-III helicity injection charge control system hardware elements.

being electrically floating for the helicity injection supplies. The control FPGA provides a frequency-modulated optical control signal representing the desired charge voltage and output state and records actuator status for the operator. The interface circuit provides the requisite frequency-to-voltage conversion and analog-to-optical-digital conversions.

Separate capacitor bank dump strategies were employed to reuse PEGASUS infrastructure where possible. Switchyard 1's dump relays are actuated by a circuit in the analog interface module. Switchyard 2's helicity injector dump system (see Fig. 1) utilizes distributed, capacitor subbank-level dump systems using optically isolated circuits, depletion MOSFETs controlled under the influence of the charge control FPGA, and dump resistors. The depletion MOSFETs allow trimming of bank voltages between shots without requiring a full discharge of the capacitors.

B. Feedback and Timing Control

A subsystem implementing in-shot timing and feedback control governs the operation of PEGASUS-III pulses. It is implemented in a PXI chassis containing a real-time embedded computer, two NI 7842R FPGA hybrid analog/digital I/O modules, an NI 7813R digital FPGA module, an NI 6683H timing module connected to a global positioning system (GPS) antenna, and ESL 6760 digital fiber-optic converters.

The feedback control subsystem is shown in relation to loads and the protection subsystem in Fig. 2(a). It implements 16 independent proportional-integral differential (PID) feedback controllers for the electromagnet and helicity injection systems that operate at control cycle loop rates up to 25 kHz. Each feedback control set samples and integrates a dedicated Rogowski coil to facilitate control of the desired load current, which is preprogrammed by a machine operator.

During a pulse, the real-time computer is responsible for sampling each feedback controller's FPGA hardware-integrated Rogowski signals, performing PID computations to determine the next control period's duty cycle, and archival of state information. FPGA modules translate the duty cycle into a command stream representing the power converter semiconductor conduction states ["C" in Fig. 2(a)] that implement the desired power converter output pulse-width modulation that also respects actuator requirements. Command stream generation is supported for one-, two-, and four-quadrant buck converters and the multi-level buck converters (MLBCs) built from IGBT and integrated gate-commutated thyristor (IGCT) power semiconductors. The FPGA modules also monitor overcurrent fault conditions ["F_{OC}" in Fig. 2(a)] and trigger a fast shutdown should they occur. Command streams from all the feedback controllers are connected to the splitter–combiner system described in the following for synchronous distribution to individual power semiconductors in the designated power supply control sets.

The timing subsystem serves several roles. First, a GPS-synchronized precision clock serves as an IEEE 1588 grandmaster for time synchronization of devices on the PEGASUS-III facility intranet. Next, it provides user-specified absolute time triggers for firing discharges at prescribed, logged times by the machine operator. During a pulse, it provides 40 general-purpose optical digital triggers with 0.1 μs precision for the facility and diagnostic systems and 15 optical triggers for piezoelectric gas valve control. Finally, it also provides five general-purpose optical digital lines for the facility that are available for use by the master facility control system.

C. Fault Protection

Two subsystems provide fault protection for the PEGASUS-III experiment. The first is a keyed interlock system located in the facility control room built entirely from digital logic circuitry and independent of computer control. It is linked to a master interlock panel in the laboratory via a fiber-optic link. All interlocks must be physically satisfied for the charge control system to permit the dump switches to be lifted and the charge actuators to energize the capacitor banks. These interlocks include: personnel keys and door entry sensors, supporting access control; emergency stop buttons; and intrashot power supply faults. In the event an interlock is not satisfied, the system latches and automatically engages the dump system to deenergize any stored energy.

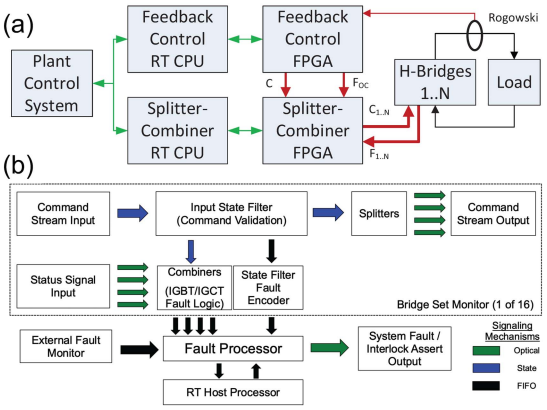

Fig. 2. (a) Block diagram of feedback control and splitter–combiner fault protection systems. (b) Detail of splitter–combiner FPGA functional elements.

The second fault protection subsystem is an FPGA-based "splitter–combiner," as detailed in Fig. 2(b). It is responsible for the validation and simultaneous distribution of command streams from the feedback controllers to power semiconductors in designated bridge modules of individual feedback control sets (splitting); continuous monitoring of power semiconductor fault status signals from the IGBT and IGCT drivers ["$F_{1..N}$" in Fig. 2(a)] and their aggregation into feedback control-set-level faults (combining); asynchronously implementing fast shutdown sequences at the feedback control set level under fault conditions that minimize the likelihood of damage to the power converter hardware; activating the facility interlock system under fault conditions; and providing attribution of detected faults to facility operators.

The splitter–combiner subsystem is implemented in a PXI chassis containing a real-time computer, two NI 7852R FPGA hybrid analog/digital I/O modules, two NI 7813R digital FPGA modules, and an NI 6672 timing module. Command stream signals are received from the feedback control subsystem via VHDCI interconnects, and optical I/O to the IGBT and IGCT switches occurs via ESL 6760 fiber-optic converters.

The splitter–combiner supports the operation of 16 independent feedback control sets. Each control set is assigned a converter topology (one-, two-, four-quadrant IGBT/IGCT, or MLBC) and a maximum number of bridge modules. Input command streams are validated to ensure that only specific switch conduction state combinations are allowed to be distributed to the devices (e.g., to avoid shoot-through); ensure that these commanded states are settled for a sufficient, semiconductor-specific temporal duration to allow all transient voltages associated with forward/reverse recovery and their handling by device- and bridge-level snubber circuitry to settle; and that only prescribed transitions between valid bridge states occur to minimize the magnitude of the switching transients and associated stresses to the power semiconductors. Minimum bridge state dwell times are reasonably bounded by 15 μs for IGBT-based converters and 25 μs for IGCT-based converters.

In the event of a fault, the splitter–combiner FPGA will initiate a fast shutdown sequence within 10 μs. All bridge sets are commanded to enter a regenerative state (no conducting switches) as soon as their minimum dwell periods have been satisfied, and the facility interlock system is activated. All faults and their relative timestamps are recorded in FPGA memory. They are relayed to the facility control system via the real-time host computer, archived with other shot data records, and presented to the operator via a virtual switch wall interface.

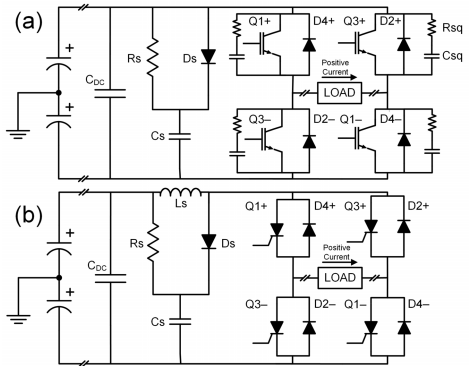

Fig. 3. Schematic of four-quadrant PEGASUS-III buck converters and snubber elements. (a) IGBT converter: $Q1\pm$: Eupec/Infineon FZ2400R17KE3 IGBT Module. $C_{\rm DC} = 937.5$ μF, $R_s = 0.65$ Ω, $C_s = 10$ μF, D_s, $D2\pm$, $D4\pm$: Dynex DSF21545SV, $R_{\rm sq} = 0.5$ Ω, and $C_{sq} = 1.5$ μF. (b) IGCT converter: $Q1\pm$ and $Q3\pm$: ABB 5SHY35L4511 IGCT module. $C_{\rm DC} = 1000$ μF, $L_s = 5$ μH, $R_s = 0.65$ Ω, $C_s = 10$ μF, D_s, $D2\pm$, and $D4\pm$: ABB 5SDF16L4503.

A prototype splitter–combiner system utilizing only FPGA-hosted protection schemes was tested during the final operational period of the PEGASUS ST. Its protections supported the final Ohmic operational research campaign (e.g., [12]) and also reduced operational costs by markedly reducing the failure/replacement rate of freewheel diodes.

IV. MODULAR BUCK CONVERTERS

The majority of controllable power for PEGASUS-III is delivered via modular buck converters that are retained or repurposed from Phase II operations of the PEGASUS Toroidal Experiment [4]. This section describes these buck converters, which were operated from 2004 to 2019, as well as a new variant on the design implemented for the PEGASUS-III toroidal field system and LHI arc systems.

A schematic for four-quadrant PEGASUS IGBT and IGCT modular buck converters is shown in Fig. 3(a) and (b), respectively. Such bridges permit bipolar current drive and regenerative current capability ($V_{\rm load} = +V, -V$) by conduction of the ($Q1+$, $Q1-$) or ($Q3+$, $Q3-$) switches. Two-quadrant converter variants are built by omitting the $Q3+$ and $Q3-$ switches. They feature unipolar current drive and regenerative capability. One-quadrant devices omit the $Q1-$, $Q3+$, $D2+$ and replace $Q1-$ and $D4-$ with a short, permitting unipolar current drive ($V_{\rm load} = +V, 0$). Switch conduction states are actuated via an optical digital command signal to a device-level driver and monitored via a digital status signal.

Representative loads for two- and four-quadrant bridges are electromagnets and helicity injector arcs; one quadrant IGCT bridges were previously employed for LHI bias [6].

Stored energy that provides $V_{\rm load}$ comes from a capacitor bank. A small local dc link capacitance is provided near the bridge module to improve the load power delivery time following changes in bridge state, compensating transmission line inductance of the bank-bridge cabling. Individual bridges are fused to limit short-circuit fault currents to 20 kA.

Snubbing circuitry is employed to mitigate switching transients associated with changes in power semiconductor conduction state. IGBT converters are snubbed by a

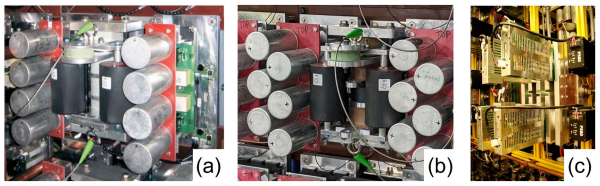

Fig. 4. Photographs of (a) 2.4 kA, 900 V IGBT; (b) 3.6 kA, 900 V IGBT; and (c) 3.5 kA, 2.7 kV IGCT buck converters. Current ratings quoted steady state.

bridge-level resistor-capacitor-diode (RCD) snubber network [R_s, C_s, and D_s in Fig. 3(a)]. Individual IGBTs are additionally snubbed at the quadrant level with *RC* snubbers [R_{sq} and C_{sq} in Fig. 3(a)]. The RCD snubber is intended to mitigate turn-off reverse-recovery voltages. IGCT converters employ an inductor-RCD (LRCD) snubber network [L_s, R_s, C_s, and D_s in Fig. 3(b)] that serves two purposes. First, it provides a turn-on current limit for the IGCT semiconductors. Second, it reduces bridge diode stresses by providing a zero-output-voltage turn-off condition, permitting safe reverse recovery. During transient suppression, the LRCD snubber has an elevated working voltage arising from absorption of the reverse recovery energy until it self-resets. This reset period is the origin of the enforced minimum dwell durations in the splitter–combiner system.

The PEGASUS IGBT buck converter [see Fig. 4(a)] is rated to provide 4.0 kA of controllable current at an operational voltage of 900 V. This rating exceeds the steady-state current rating of the IGBTs (2.4 kA) but is permissible due to the pulse lengths of the experiment. A new variant of the converter using 3.6 kA IGBT modules (equivalent to Fig. 3(a), with $Q\{1, 3\}\pm$, $D\{2, 4\}\pm$ ABB 5SNA3600E170300; $C_{\text{DC}} = 1875\ \mu$F) has been developed for PEGASUS-III operation [see Fig. 4(b)] that extends the working pulse length and dc current rating.

The PEGASUS IGCT buck converter [see Fig. 4(c)] is rated for 3.5 kA of controllable current and a working voltage up to 2.7 kV. The IGCTs, however, carry a much higher surge current rating, provided that it is only interrupted below the ∼3.5 kA level, making the devices suitable for other applications such as crowbars.

V. HELICITY INJECTOR MULTI-LEVEL BUCK CONVERTER

A new multi-level buck converter is implemented to support PEGASUS-III helicity injector operation. These sources require unipolar current drive, $I_{\text{inj}} \sim 4$ kA/source, high working voltage $V_{\text{inj}} \geq 1$ kV, and have a time-varying impedance set by plasma parameters internal and external to the injectors [6], [13]. In addition, for proper biasing, the power supply for these sources must be electrically floating.

The new converter is comprised of a 900 V, two-quadrant IGBT module under feedback control placed in series with an unregulated 1800 V, two-quadrant IGCT module. An output silicon-controlled rectifier (SCR) crowbar is additionally provisioned in the converter to support rapid (∼100 μs) injector shutoff for physics studies. The capacitor banks for each level are capable of independent operating voltages. This configuration allows for a nominal +1.8 kV dc applied from

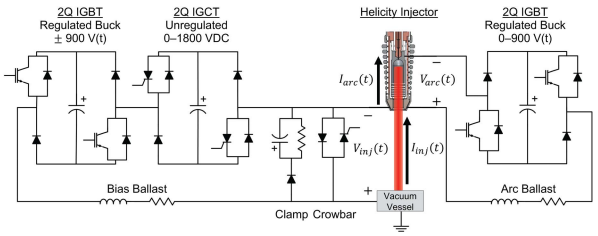

Fig. 5. Schematic and nominal working voltages of PEGASUS-III multilevel buck converter (left), helicity injector and protection circuits (center), and arc supply (right) configured for LHI operation.

the IGCT level, corrected by ±900 V(t) on sub-millisecond timescales from the IGBT level. Under fault conditions, the MLBC can additionally apply regenerative drive in the IGCT stage to reduce load current more rapidly.

Fig. 5 shows the MLBC bias supply, IGBT arc supply, and helicity injector circuitry associated with drive of a single injector. A two-quadrant IGBT bridge drives an arc current interior to the (electrically isolated) helicity injector. The injector is biased negatively to the vacuum vessel by the MLBC supply to extract an electron current. The arc and bias currents are stabilized by a series ballast resistance and inductance. An RCD clamp serves to reduce additional output voltage ripple.

VI. ZERO-VOLTAGE-SWITCHING RESONANT CONVERTER

The DNB and RF sources for PEGASUS-III require high voltage (60–80 kV), low current (5–10 A), low ripple (<0.5%–2%), very low energy transfer to the load under fault conditions (<5 J), and pulse length ∼0.1 s. A ZVS resonant converter (see Fig. 6) is under development to address these requirements. It functions by driving a tuned resonant *LC* circuit near its resonance with a three-phase variable frequency drive. Selecting the drive frequency specifies the output gain of the converter. Its resonance is designed to be near 45 kHz, which permits reduction of the amount of stored energy in the high-voltage stage and reduces the physical size of the system.

Fig. 6(a) shows the high-level design of the converter. A three-phase dc–ac inverter stage drives a resonant *LC* transformer circuit for each phase near its resonant frequency. The transformers generate high-voltage ac, which is rectified and filtered by a shunt capacitor. The filtered, high-voltage dc output is current limited and delivered to the load via coaxial cabling. A core snubber provides additional load protection during faults.

The low-voltage stage of the ZVS converter [see Fig. 6(b) and (d)] is comprised of three half-bridge inverters powered by 120 kJ of stored energy in center-point grounded, 3.6 kV capacitor banks. The LRCD snubber network [$\{L, R, C, D\}_{X\pm}$ in Fig. 6(b)] substantially reduces IGBT turn-on and turn-off switching losses by zeroing the device voltage during transitions for ∼1 μs [14]. This permits each phase to operate at ∼30 kHz for a 0.1-s pulse. Absent the snubber, operations would be thermally limited to <5 ms. This operating point allows useful voltage gain (∼20–30×) that can also compensate capacitor droop during a long pulse. The three-phase configuration effectively multiplies the working ripple frequency by a factor of six.

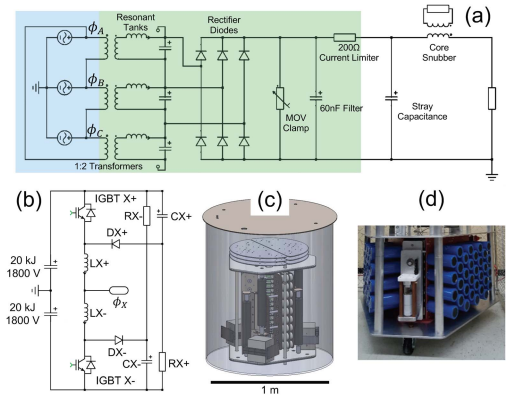

Fig. 6. Schematic of PEGASUS-III ZVS resonant converter. (a) High-voltage stage. (b) Detail of single phase in low voltage inverter and its energy supply. IGBT, freewheel D: ABB 5SNA 0650J450300, DX: Dean/HVCA JB511, LX: 2 μH, RX: 1 Ω, and CX: 0.5 μF. (c) CAD of high-voltage stage in dielectric. (d) Photograph of low-voltage dc–ac inverter stage.

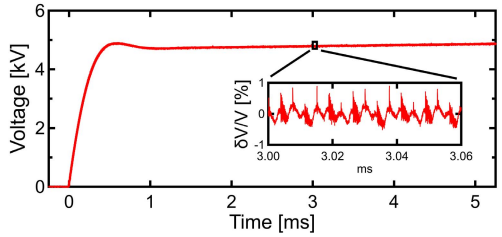

Fig. 7. 5 kV test of ZVS converter. Peak–peak (rms) ripple <1.7 (0.2)%.

The high-voltage stage [see Fig. 6(c)] is comprised of passive elements and immersed in FR3 dielectric fluid to facilitate operation at high voltage in a compact volume. Ripple in the rectified phases is reduced by careful balancing of the resonant capacitances in Fig. 6(a), which are constructed from multiple high-voltage capacitors in parallel/series configuration.

The loads driven by this system are easily damaged by arcing and accordingly must be protected to the extent possible. The high operating base frequency on the low voltage stage limits the stored energy in the high voltage stage. The high-frequency ripple on the dc output is readily filtered by a small high-voltage capacitor. This enables fast fault response and simple, passive fault protection systems. An inductively coupled core snubber is also being implemented to absorb high-frequency energy arising from arc faults. It employs a similar design used on the EAST neutral beam sources [15], [16] using Finemet and Deltamax tapes to balance frequency response and the available fault energy absorption capability.

The ZVS resonant converter has been tested up to 35 kV in air with satisfactory performance. Fig. 7 shows a representative pulse from the converter with 0.2% rms ripple. Individual phase ripple is consistent with PLECS modeling of the converter using measured system parasitic inductances and capacitances. The 1.7% worst case peak–peak ripple shown here is acceptable for a DNB application. However, further improvement is required for driving RF sources. This may be straightforwardly achieved with improved balancing of the rectifier capacitance and its filtering.

VII. Conclusion

A variety of power systems have been developed to support the initial operation of the PEGASUS-III experiment. 7 MJ of new stored energy backs ∼175 MVA of controllable power for the facility. Successful buck converter designs from PEGASUS are being expanded and modernized for electromagnet drive, and new MLBCs are being fielded for the helicity injectors. These systems are controlled and protected by fully digital systems using real-time computing and FPGA technology. Transient CHI will be supported by a new low-inductance capacitor bank. A ZVS converter provides high voltage, low ripple current for the DNB and appears suitable for adaptation to RF sources.

Acknowledgment

Disclaimer: Any opinions, findings, and conclusions or recommendations expressed in this publication are those of the authors and do not necessarily reflect the views of the U.S. Department of Energy. Data from this publication are publicly available in openly documented, machine-readable formats [17].

References

[1] J. E. Menard *et al.*, "Fusion nuclear science facilities and pilot plants based on the spherical tokamak," *Nucl. Fusion*, vol. 56, no. 10, Oct. 2016, Art. no. 106023, doi: 10.1088/0029-5515/56/10/106023.

[2] J. E. Menard, "Compact steady-state tokamak performance dependence on magnet and core physics limits," *Phil. Trans. Roy. Soc. A: Math., Phys. Eng. Sci.*, vol. 377, no. 2141, Mar. 2019, Art. no. 20170440, doi: 10.1098/rsta.2017.0440.

[3] R. Raman and V. F. Shevchenko, "Solenoid-free plasma start-up in spherical tokamaks," *Plasma Phys. Controlled Fusion*, vol. 56, no. 10, Oct. 2014, Art. no. 103001, doi: 10.1088/0741-3335/56/10/103001.

[4] G. D. Garstka *et al.*, "The upgraded pegasus toroidal experiment," *Nucl. Fusion*, vol. 46, no. 8, pp. S603–S612, Jul. 2006, doi: 10.1088/0029-5515/46/8/s06.

[5] A. C. Sontag *et al.*, "The new PEGASUS-III experiment," *IEEE Trans. Plasma Sci.*, to be published.

[6] M. W. Bongard *et al.*, "Advancing local helicity injection for non-solenoidal tokamak startup," *Nucl. Fusion*, vol. 59, no. 7, Jul. 2019, Art. no. 076003, doi: 10.1088/1741-4326/ab17e3.

[7] T. R. Jarboe, "Formation and steady-state sustainment of a tokamak by coaxial helicity injection," *Fusion Technol.*, vol. 15, no. 1, pp. 7–11, Jan. 1989, doi: 10.13182/fst89-1.

[8] R. Raman *et al.*, "Transient coaxial helicity injection for solenoid-free plasma startup in HIT-II," *Phys. Plasmas*, vol. 14, no. 2, Feb. 2007, Art. no. 022504, doi: 10.1063/1.2437115.

[9] J. A. Reusch *et al.*, "A coaxial helicity injection system for non-solenoidal startup studies on the PEGASUS-III experiment," *IEEE Trans. Plasma Sci.*, to be published.

[10] M. W. Bongard, R. J. Fonck, B. T. Lewicki, and A. J. Redd, "A Hall sensor array for internal current profile constraint," *Rev. Sci. Instrum.*, vol. 81, no. 10, Oct. 2010, Art. no. 10E105, doi: 10.1063/1.3475539.

[11] H. W. Ott, *Electromagnetic Compatibility Engineering*, 1st ed. Hoboken, NJ, USA: Wiley, 2009.

[12] G. M. Bodner *et al.*, "Initial characterization of electron temperature and density profiles in PEGASUS spherical tokamak discharges driven solely by local helicity injection," *Phys. Plasmas*, vol. 28, no. 10, Oct. 2021, Art. no. 102504, doi: 10.1063/5.0054974.

[13] E. T. Hinson, J. L. Barr, M. W. Bongard, M. G. Burke, R. J. Fonck, and J. M. Perry, "Impedance of an intense plasma-cathode electron source for tokamak startup," *Phys. Plasmas*, vol. 23, no. 5, May 2016, Art. no. 052515, doi: 10.1063/1.4952628.

[14] S. J. Finney, D. J. Tooth, J. E. Flethcer, and B. W. Williams, "The application of saturable turn-on snubbers to IGBT bridge-leg circuits," *IEEE Trans. Power Electron.*, vol. 14, no. 6, pp. 1101–1110, Nov. 1999, doi: 10.1109/63.803404.

[15] F. Xie, G. Li, D. Cheng, and Q. Chen, "Analysis and application of the series core snubber," *Plasma Sci. Technol.*, vol. 15, no. 5, pp. 469–475, May 2013, doi: 10.1088/1009-0630/15/5/15.

[16] C.-C. Jiang *et al.*, "Development of a core snubber for the neutral beam injector on EAST," *Rev. Sci. Instrum.*, vol. 87, no. 12, Dec. 2016, Art. no. 123302, doi: 10.1063/1.4972883.

[17] M. W. Bongard *et al.*, "Public data set: Digital control and power systems for the PEGASUS-III experiment," doi: 10.18138/1834594.